CONTROL LAW SYNTHESIS AND WIND TUNNEL TEST OF GUST LOAD ALLEVIATION FOR A TRANSPORT-TYPE AIRCRAFT

H. Matsushita*, T. Ueda,**K. Fujii†, Y. Miyazawa,††M. Hashidate‡and Y. Ando§

National Aerospace Laboratory, Tokyo, Japan

Abstract

In this paper, a systematic control law synthesis method for active control of an aeroelastic aircraft and dynamic wind tunnel test results using an active model-suspension system are described. A scaled model of a transport-type aircraft, which has a flexible wing with aeroelastic similarity, was designed and constructed. The math model was derived in the state space form based on finite element structural analysis coupled with boundary element aerodynamic analysis. Practical low order control laws for gust load alleviation were synthesized by applying the LQG optimal control law synthesis method with the order reduction procedure. The control law thus obtained was implemented in the digital computer and tested in the 6.5m X 5.5m low speed wind tunnel at the National Aerospace Laboratory. Using a newly developed active model-suspension system, the model was supported so as to give freedom of heaving and pitching motions. The test verified that the optimal reduced order control law could effectively suppress the rigid-body motion contribution, as well as the flexible wing contribution, to the wing bending moment.

1. Introduction

Active control technology of aircraft, especially for aeroelastic system oriented, is one of the most promising technologies for bringing about a new era of fully integrated vehicles. Ever since the pioneering manuscript written by Bisplinghoff et al predicted the possibility of actively controlling flutter,[1] research efforts on this active aeroelastic control have been carried out over a wide range, from basic researche on active flutter suppression to practical developments on gust response reduction. Owing to the intensive theoretical research activities carried out by many researchers ever since, the method of state space math modeling and synthesis of an optimal full-state full-order output control law based on this method are well developed. We can now estimate to what extent a certain aeroelastic system can be improved by an optimal feedback control. Before this optimal feedback control into practical use, however, research must be conducted on methods to get practical, low order control laws which can easily be implemented in an onboard computer.

In the area of experimental investigation in wind tunnel tests, there have been also steady efforts all over the world. To name a few, the research activity[2] of NASA Langley RC in its Transonic Dynamic Tunnel is one of the most profound of all, and the intensive research, named GARTEur project, executed by European countries, is also a fruitful activity.[3-5] Among these continuous research activities have been our own investigations.(Fig.1)[6-12] Previous wind tunnel studies show that our methods of synthesis are useful in designing an active aeroelastic control system, specifically gust load alleviation for high aspect-ratio wing[7,10] and active flutter control of both a single-use control surface[8,11] and multi-use of leading- and trailing-edge control surfaces.[12,13]

We have extended our verification study to a complete aircraft model, utilizing the wing used in the previous test as its right wing. To this aircraft model, the LQG optimal control law synthesis method was applied. Hyland's order reduction procedure[14] was further carried out to obtain practical low order control laws.

The control law thus obtained was tested in the 6.5m X 5.5m low speed wind tunnel at the National Aerospace Laboratory. This paper describes these analytical and experimental results.

2. Aircraft Model Construction

A scaled aircraft model for wind tunnel test was constructed. Since the objective of the present research is focused on the effect of the body freedom motion to gust load alleviation due mainly to the wing flexibility, it was decided to construct a model with rigid body and flexible wing. The wing used in the previous serial experiment was adopted as the right wing of the model. The three way view of the model is shown in Fig.2 and the principal dimensions of the model are described in Table 1. Fig. 3 shows the model aircraft in the wind tunnel test section executing the gust load alleviation experiment. The model wing has aeroelastic similarity to a certain future transport aircraft. It has an aluminium alloy spar simulating stiffness characteristics. A total of 15 wing segments of NACA0012 section are attached to it for each wing. More details of the wing configuration can be found in Ref. 12. Accelerometers are installed at the right and left wing spars towards the inboard side of the trailing-edge control surfaces (designated as AR and AL in Fig. 2). The strain gages for measuring bending(E3, E4) and torsional (E1, E2) deformation are also placed on a wing spar. The right and left ailerons are driven separately by an electric DC servo-motor through a gear train. In order to measure the rigid body motion, accel-

*Senior Researcher, Advanced Aircraft Research Group
**Head, Flight Load Branch, Airframe Division
†Researcher, Advanced Aircraft Research Group
††Senior Researcher, Flight Research Division
‡Senior Researcher, Aircraft Aerodynamics Division
§Senior Researcher, Airframe Division

erometers are attached fore and aft of the model body (AF, AA). The elevator is driven through a wire cable by a stepping motor placed on the aft body stringer.

The acceleration signals and/or bending strain signals are charged to an analogue or digital computer which is installed outside the wind tunnel test section. The computer implements a control law which generates driving feedback signals to the actuators so that the control system may alleviate the wing root bending moment.

3. Mathematical Modeling

3.1 Fundamental Equations

In order to synthesize control laws by applying the optimal control theory for a lumped parameter system, a mathematical model of an aircraft in the form of state space should be derived. The math model of the present aircraft model is derived by the same procedure as for our cantilevered wing model. We derive the math model by the modal approach for structural dynamics and by the finite dimensional approximation for unsteady aerodynamics. We describe it here briefly, emphasizing the specific feature to the complete aircraft model. For more details of the procedure for dealing with the wing flexibility, the reader should refer to Refs.7 or 9.

For the aircraft model with flexible wing, the equation of the motion may comprise the rigid body motion, the flexible wing vibration and the control surface actuator dynamics. Neglecting the inertial coupling terms of the wing and the control surfaces for rigid-body motion, the equations for longitudinal symmetrical motion can be written as,

For rigid-body heaving motion :

$$m\ddot{h} = L_\alpha \alpha + L_{\dot\alpha}\dot\alpha + L_q q + \sum_{i=1}^{N}\{L_{q_i} q_i + L_{\dot q_i}\dot q_i\} + L_\alpha \alpha_g + L_{\delta a}\delta_a + L_{\delta e}\delta_e \quad (1a)$$

For rigid-body pitching motion :

$$I_y\ddot\theta = M_\alpha \alpha + M_{\dot\alpha}\dot\alpha + M_q q + \sum_{i=1}^{N}\{M_{q_i} q_i + M_{\dot q_i}\dot q_i\} + M_\alpha \alpha_g + M_{\delta a}\delta_a + M_{\delta e}\delta_e \quad (1b)$$

where m and I_y are the mass and the moment of inertia of the model, respectively. $\alpha = \theta - \dot h/u_0$ is angle of attack, q is pitch rate, and q_i's are the generalized coordinates for wing elastic modes. α_g is gust incident, δ_a aileron deflection, δ_e elevator. L_α's and M_α's are quasi-steady aerodynamic coefficients.

The equation of the wing vibration can be expressed as :

$$\frac{1}{\omega_i^2}\ddot q_i + \frac{2\zeta_i}{\omega_i}\dot q_i + q_i + s_{ai}\ddot\delta_a + s_{ei}\ddot\delta_e = f_i(t) \quad (1c)$$
$$; \ i = 1, \cdots, N$$

where the 4th and 5th terms on the left hand side of Eq.(1c) present the inertial coupling effects. The generalized aerodynamic forces on the right hand side of Eq.(1c) can be expressed in the same manner as in the cantilevered wing with the aerodynamic lag terms :

$$f(t) = \left(\frac{b}{u_0}\right)^2 A_2 q + \left(\frac{b}{u_0}\right) A_1 q + A_0 q + z$$
$$\left(\frac{b}{u_0}\right)\dot{\mathbf{z}} = \mathbf{F}\mathbf{z} + \mathbf{G}\mathbf{q}, \ \mathbf{z} \equiv R^N \quad (2)$$

where $\mathbf{q} = (q_1\ q_2\ \cdots\ q_N)^T$, $\mathbf{F} = \mathrm{diag}\{-\lambda, \cdots, -\lambda\}$

With this expression incorporated into Eq.(1c) and taking account of the system noise $\mathbf{w}(t)$, we obtain the standard formulation of the state equation of motion. The equations for control surface actuating systems can be expressed by 2nd order dynamic systems as,

$$\frac{1}{\omega_{\delta m}^2}\ddot\delta_m + \frac{2\zeta_{\delta m}}{\omega_{\delta m}}\dot\delta_m + \delta_m = \delta_{cm} \quad ; \ m = a, e \quad (1d)$$

In Eq.(1b), δ_{cm}'s are control surface command; m=a for an aileron and m=e for an elevator. As for the elevator, eq.(1d) presents the rate limiting circuit which is placed prior to the stepping motor in order not to be disordered due to unintentional jump in the command signal.

The final state form of equation can thus be summarized by Eqs.(1a),(1b),(1c) and (1d) as,

$$\dot{\mathbf{x}} = \mathbf{A}\mathbf{x}(t) + \mathbf{B}\mathbf{u}(t) + \mathbf{w}(t) \quad (3)$$

where $\mathbf{x} = (\dot h, \dot\theta, \dot{\mathbf{q}}, h, \theta, \mathbf{q}, \mathbf{z})^T$, $\mathbf{u} = (\delta_{ca}, \delta_{ce})^T$.

As we have two sets of sensors, one for acceleration **a** and the other for strain ε, we can derive the output equation expressing it with the state and control variables in Eq.(3). The standard form of output equation can be expressed with measurement noise $\mathbf{v}(t)$ taking part, as

$$\mathbf{y} = \mathbf{C}\mathbf{x}(t) + \mathbf{D}\mathbf{u}(t) + \mathbf{v}(t) \quad (4)$$

where $\mathbf{y} = (\mathbf{a}, \varepsilon_B)^T$.

3.2 Data Acquisition for Math Model

In order to determine the coefficients in Eqs.(3) and (4), we have carried out two sets of tests: ground vibration tests for structural dynamics and wind tunnel tests for aerodynamics. Supplementally, we have measured the acceleration response of the wing due to the aileron random excitation.

Ground Vibration Test and FEM Analysis. Table 2 summarizes the results obtained by the series of ground vibration tests; symmetrical and anti-symmetrical excitation, swept-sine and random excitation.[15] We can identify a total of seven modes, symmetrical and anti-symmetrical, over the frequency range of interest up to 20 Hz. Fig.4 shows some typical test results of the 1st and 2nd bending modes. The aileron excitation results are shown in Fig.6. We can observe in Table 2 and

Fig.6 that the torsional modes lack in symmetry. The lower frequency mode is dominated by left wing deflection, while the higher frequency mode is dominated by right wing deflection. Since the right wing had experienced flutter so many times during the previous flutter control tests, there might be a slight difference in the stiffness characteristics between the two wings. We have derived the symmetrical mathematical model from these non-symmetrical models as will be stated later.

We conducted FEM analysis for this model aircraft.[15] The analysis results are also shown in Table 2, Fig.4 and Fig.5. These results show good agreement between the test and analysis. Using these results, we constructed the structural math model with natural frequencies from test data and mode shapes from the FEM analysis.

Wind Tunnel Tests and Static Aeroelastic Analysis. In order to offer the quasi-static data and confirm the equilibrium trimmed condition, we executed a static wind tunnel test[16] and computational aeroelastic analysis.[17] Fig.7 shows the results of the test. Because of the flexibility of the wing, we obtained different aerodynamic coefficients according to the wind velocity; smaller C_L values were obtained for higher velocities.

For executing static aeroelastic analysis, we combined the aerodynamic computer cord of the boundary element method with the structural analysis cord of the finite element method. We used iteratively these two sets of algorithms to reach the final results. The model aircraft was assembled from the six subcomponents shown in Fig.8(a) in order to apply the aerodynamic cord. The wireframe of the model for computation is shown in Fig.8(b). By taking the wing flexibility into account , we can more precisely predict the test results than through rigid body analysis. Fig.9 presents some typical pressure distributions obtained by this static aeroelastic analysis. In Table 3 are shown lift curve slope values obtained by the test and the analysis.

3.3 Mathematical Model Construction

Taking these preceding test results into the fundamental equations stated previously, we obtain the mathematical model. We derived two different kinds of math model; one is a more sophisticated model which can predict test results better than the other model. This model is to be used as the basis to evaluate the control laws obtained prior to the experiment. The other model is symmetrical and of lower order one and is to be used as the controlled plant for designing the control law. The former is of order 24. It incorporates two degrees of rigid body motion, five degrees of wing elastic vibration, two sets of actuator dynamics and a gust generating filter. It also incorporates the five augmented state variables representing the aerodynamic lag effect for each elastic mode.

Since we are to treat longitudinal motion and vibration, we have to construct a symmetrical structural model. At this stage we have a problem of how to get a symmetrical mathematical structural model from GVT data which is not strictly symmetrical. We have carried out root locus analysis using the 24th order model just obtained and examined whether it can appropriately predict aeroelastic instability characteristics. Fig.10(a) shows the analytical results where the left wing torsion mode goes into an unstable state. We decided to take the left wing torsional stiffness symmetrized to the right wing so as to obtain the symmetrical math model. We have the symmetrical math model of the least order of 18 necessary to predict aeroelastic instability. In Fig.10(b) is shown the velocity root locus of this symmetrized model which can predict aeroelastic instability with good agreement to the 24th order model.

4. Control Law Synthesis

4.1 Optimal Control Design

Now that we have obtained the math model, we can apply the LQG control theory and obtain the optimal control laws. The synthesis procedure is illustrated in Fig. 11. Since the present purpose of our gust load alleviation study is to examine the effect of the rigid body motion on the reduction of the the wing root bending moment, we choose the elastic energy incorporated in the nominal cost function. For the purpose of comparison, we also choose the different set of the performance index which includes the dynamic energy of the rigid-body motion. The cost function can be uniformly defined for both cases using kinetic energy plus control cost as follows.

$$J = E\{\frac{1}{2}x^TQx + \frac{1}{2}u^TRu\} \tag{5}$$

Since the velocity root locus predicts that aeroelastic instability will occur at just above 30 m/s, we set the design speed at 25 m/s.

Full-state perfect measurement control. The first step of the synthesis procedure is to design the full-state perfect measurement feedback control law by fixing the weights in the cost function. With the weights as a parameter, we solve the following matrix Riccati equation.

$$AP^T_1 + P_1A - P_1BR^{-1}B^TP_1 + Q = 0 \tag{6}$$

Feedback control of an optimal regulator can be expressed with the solution to this equation as

$$K_1 = R^{-1}B^TP_1 \tag{7}$$

We can thus obtain an energy diagram as a function of aileron and elevator deflections in rms value with control weights as parameters. Figs.12 shows this energy diagram as a bird's-eye view. Note that elevator axis is double the aileron axis. Fig.12(a) shows the elastic component versus the total energy where the cost function includes the dynamic energy of the rigid-body motion. The Figure shows that the rigid-body component of the total energy, shown as the upper portion, is little affected by either control surface. The effect of inclusion of the rigid-body motion energy in the cost function is shown in Fig. 12(b). Since it is more effective to evaluate the elastic energy than to include the rigid-body contribution, the cost function is set to exclusively comprise the elastic

energy. As can be seen in the Figure, the system energy increases as we try to save control cost. We, therefore, have to trade off control cost and energy. We set the design weights as (20, 20) as shown in Fig. 12(b), where we have enough alleviation of the elastic energy reserving the margin of the degradation of the control effectiveness throughout the control design procedure.

Fig.12(c) shows the dominant contribution of the 1st bending moment to total energy reduction. This situation is the same as for the cantilevered wing.

Full-order output controller. Since we can approach the state of the controlled plant only through the sensor output, we have to estimate the state variables from these outputs. An output controller with a state estimator has to be synthesized. We choose the two sets of the sensor output. One is the acceleration and the other is the acceleration plus the bending strain. To design the LQG observer, the system noise level and the measurement noise level are needed. The measurement noise levels are set to 0.5 m/sec^2 in rms value for acceleration and 1.0 Nm rms for bending strain. As for system noise, 0.25 deg rms of the control surface deflection is introduced. With these numerical values, we can solve another matrix Riccati equation of the form:

$$AP_2 + P_2A^T - P_2C^TV^{-1}CP_2 + W = 0 \qquad (8)$$

and the Kalman estimator can be obtained as

$$K_2 = P_2C^TV^{-1} \qquad (9)$$

The order of the control laws thus obtained is 18 which is the same as the plant math model.

The estimation of the state degrades the control performance at some degree. As shown in Table 4, in case of the acceleration feedback, 44.7% reduction of the elastic energy for full state feedback is degraded to 41.7%, while inclusion of the bending strain signal improves the value to 42.6%.

4.2 Reduced Order Output Controller

Since a full order controller of 18th order is still too high to be implemented in a computer in a real time sense, order reduction is necessary. We cannot incorporate an excessively high order control law in the computer, while there might be some state variables in the control law which make a lesser contribution to the control performance.

As order reduction procedure we here adopt Hyland's method.[14] For acceleration feedback, the original 18th order filter is eventually reduced to 2nd order, while for acceleration plus bending strain, we can obtain a final order of five. These low order filters can easily be implemented by an analogue computer in experiments. As for the previous study of flutter control for the cantilevered wing by leading edge and trailing edge control surfaces, the original 16th full order controller could not be reduced to more than the 6th order. We have succeeded in order reduction as low as the 2nd order probably because the coupling of the two control surfaces is not so close as for flutter control.

In Fig. 13 is shown the energy level trend vs. the reduced order. Table 4 summarizes the control performance for these optimal reduced order controllers. As can be seen in this Figure and Table, though order reduction degrades the control performance to some extent, these values still fulfill the specified design objective.

5.Wind Tunnel Test

In order to verify the effectiveness of the control law, we conducted a wind tunnel test. Fig.14 and the picture in Fig.15 show the testing set-up of the gust load alleviation experiment carried out in the 6.5m X 5.5m low speed wind tunnel of the National Aerospace Laboratory.

Active Suspension System. As the textbook of Bisplinghoff et al[1] points out, there are some difficulties in conducting a dynamic simulation test in a wind tunnel which satisfies both aeroelastic and dynamic similarity. For a model which already meets the aeroelastic similarity requirement, the model lift is insufficient to support its weight in a low speed test. In the high speed test, the situation is reversed. Our model is no exception. We need some device for yielding constant supporting force in spite of the model motion so that the model can fly unrestrained in the tunnel.

We have developed a supporting system which can meet these requirements. A picture of the system is shown in Fig.16. The model is supported by and can move along the vertical rod. It also has pitch freedom. The vertical force is supplied by the two supporting wire cables, whose tension is kept constant, controlled by the torque motor attached to the wind tunnel test section. The system can exert an arbitrarily adjusted supporting force so that we can execute dynamic wind tunnel tests at various trimmed speed conditions. This system can also exert restoring force and damping force, the amount of which can be set appropriately according to the test conditions. The system can also prevent excessive vertical velocity of the model so that it will be damaged. The essential part of the system dynamic compensator is depicted in Fig.17 and the frequency response of the system is shown in Fig.18. It can be seen in Fig.18 that the disturbing force to the system is well damped through a wide range of lower frequencies.

Control Law Implementation. The control laws which we installed in the tests are 2nd and 4th order control laws for acceleration feedback, 5th order control law for acceleration plus bending strain feedback. These optimal reduced order controllers were implemented in a digital computer.

For the purpose of comparison, a 1st order filter was also implemented in the test. This control law was prepared to produce the damping force to the wing vibration, especially effective to its 1st bending mode. Its cut-off frequency lies at a very low value of 0.1 Hz so that it is expected to act as damping for almost every frequency range of interest. This control law was

implemented in an analog computer.

Experimental results are summarized in Table 5 and Fig.19 where these two different control laws are compared. In frequency ranges above 1 Hz, where the rigid-body motion is excluded, the 1st order damping control works as expected. For the full frequency range, however, its total performance is poor due to the large negative effect in the frequency range of the rigid-body motion. On the other hand, the optimal reduced order controller can work as well over the whole range as in the elastic mode range. These results confirm that the LQG control synthesis procedure with an order reduction method is also very useful for active aeroelastic control.

6. Conclusions

A new wind tunnel testing technique using an active suspension system has been developed for gust load alleviation experiments. Throughout the speed regimes, this technique makes it easy to meet requirements not only for aeroelastic similarity but rigid body motion similarity as well.

This active suspension system is used in a gust load alleviation experiment for a transport-type aircraft model. The system can supply a constant supporting force to the model regardless of its motion where the lift in its designed trim condition is not sufficient to support the model weight.

Practical low order control laws for gust load alleviation were synthesized by applying the LQG optimal control theory with an order reduction procedure and were verified effective in wind tunnel tests.

Acknowledgment

The authors would like to express their sincere appreciation to those in NAL who contribute to the wind tunnel experiment. Especially, their thanks extend to Mr. T. Kikuchi for developing the model tail assembly with its control surface driving mechanism and to Mr. S. Suzuki for developing the gust generating device. The development of the active model-suspension system was conducted as cooperative works with Shin Meiwa Industry Co.,Ltd.

Table 1 Principal Dimensions of ACT Aircraft Model

Length	4.02 m	Aspect Ratio	9.86
Span	3.40 m	Awept Back Agl	18 deg
Height	0.95 m	Wing Incidence	5.85 deg
Weight	40.4 Kg	Dihedral Angle	3 deg
I_y	38.83 Kgm^2	Taper Ratio	0.3
		Elastic Axis	40% Wing Chord

Table 2 Elastic Modes of ACT Aircraft Model

Static Aeroelastic Analysis				Wind Tunnel Test
Rigid-Body	Bending 25 m/s	B/Torsion 20 m/s	B/Torsion 25 m/s	25 m/s
5.78	4.66	4.96	4.69	4.86

Table 3 Test and Analysis Results of Lift-Curve Slope

	Uncontrolled Aircraft	Full State Feedback	Accel. Feedback			Accel. & Bending	
			Full Order	4th Order	2nd Order	Full Order	5th Order
Elastic Energy, N	1.209	0.681	0.705	0.790	0.845	0.695	0.756
Reduction Ratio	1.000	0.563	0.583	0.653	0.699	0.574	0.626

References

1 Bisplinghoff, R.L., Ashley, H. and Halfman, R.L., "Aeroelasticity," Addison-Wesley Publishing Co., 1955.

2 Noll, T., Perry, B., III, and Gilbert, M., "Recent Activities within the Aeroservoelasticity Branch at the NASA Langley Research Center,"Proceedings of the European Forum on Aeroelasticity and Structural Dynamics, Aachen, FRG, April 17-19, 1989, pp.509-517.

3 Destuynder, R. and Honlinger, H., "Multi-Control System in Unsteady Aerodynamics using Spoilers," AIAA Paper No.87-0855.

4 Destuynder, R., Gravelle, A. and Legrain, I., "Simultaneous Active Controls on Wind Tunnel Model," ONERA RA 1987-2.

5 Gelder, P.A., "Design of an Integrated Control System for Flutter Margin Augmentation and Gust Load Alleviation, Tested on a Dynamic Windtunnel Model," NLR MP 86034 U.

6 Matsushita, H., "Active Aeroelastic Control - Research Status in NAL," Journal of the Japan Society for Aeronautical and Space Sciences, Vol. 35, No.3, 1987, in Japanese.

7 Matsuzaki, Y., Ueda, T., Miyazawa, Y. and Matsushita, H., "Gust Load Alleviation of a Transport-Type Wing: Test and Analysis," Journal of Aircraft, Vol. 26, April 1989, pp.322-327.

8 Ueda, T., Matsushita, H., Suzuki, S., Miyazawa, Y. and Matsuzaki, Y., "ACT Wind Tunnel Experiments of a Transport-type Wing," ICAS '88, Israel, Aug. 28 - Sept. 2, 1988.

9 ACT Study Group, "Gust Load Alleviation of a Cantilevered Rectangular Elastic Wing. -- Wind Tunnel Experiment and Analysis." NAL TR-846, 1984, in Japanese.

10 ACT Study Group, "Wind Tunnel Tests and Analysis on Gust Load Alleviation of a High-Aspect-Ratio Wing," NAL TR-890, 1985, in Japanese.

11 ACT Study Group, "Wind Tunnel Tests on Flutter Control of a High-Aspect-Ratio Cantilevered Wing, 1st Report," NAL TR-978, 1988, in Japanese.

12 Matsushita, H., Miyazawa, Y., Ueda, T. and Suzuki, S., "Multi-Surface Control Law Synthesis and Wind Tunnel Test Verification of Active Flutter Suppression for a Transport-Type Wing," Proceedings of the European Forum on Aeroelasticity and Structural Dynamics, Aachen, FRG, April 17-19, 1989, pp.519-527.

13 ACT Study Group, "Wind Tunnel Tests on Flutter Control of a High-Aspect-Ratio Cantilevered Wing, 2nd Report," to appear as NAL TR, 1990, in Japanese.

14 Yousuff, A. and Skelton, R. E., "Controller Reduction by Component Cost Analysis," IEEE Trans. on Autom. Contr., Vol.AC-29, No.6, 1984, pp.520-530.

15 Ueda, T., Fujii, K. and Ando, Y., "On the Vibration Test of ACT Aircraft Wind Tunnel Model and Its Mathematical Modeling," Proceedings of the Annual Conference of the Japan Society for Aeronautical and Space Sciences, April, 1988, pp.83-84, in Japanese.

16 Suzuki, S., Murota, K., et al, "Static Aerodynamic Test of NAL ACT Aircraft Model with Flexible Wing," Proceedings of Aircraft Symposium, the Japan Society for Aeronautical and Space Sciences, Oct. 1988, pp.520-523, in Japanese.

17 Matsushita, H., Fujii, K., Ueda, T. and Yanagisawa, M, "Static Aeroelastic Analysis of ACT Wind Tunnel Model Aircraft," to appear as NAL TM, 1990, in Japanese.

Table 4 Elastic Energy Reduction Estimated with Optimal Control

Flexible Modes	GVT Results	FEM Analysis
1st Wing Bending	2.25	2.20
1st Wing Bending(Anti)	2.58	2.60
2nd Wing Bending	7.44	8.65
2nd Wing Bending(Anti)	7.84	8.85
Left Wing Torsion	11.50	11.50
Right Wing Torsion	13.30	13.30
3rd Wing Bending	14.50	16.99

Table 5 Experimental Results of GLA, Gust Response Reduction Ratio

Control Law		20m/s 0~20Hz	20m/s 1~20Hz	25m/s 0~20Hz	25m/s 1~20Hz
A1[a]	BM[c]	1.585	0.648	2.621	0.566
	Acc[d]	0.951	0.678	0.952	0.600
RA1[b]	BM	0.721	1.016	1.028	0.756
	Acc	1.304	1.152	0.681	0.638

a A1 : Wing Deflection Rate Feedback (1st order)
b RA1 : Optimal Reduced Order Control (2nd order, design velocity = 25m/s)
c BM : Bending Moment Reduction Ratio
d Acc : Acceleration Reduction Ratio

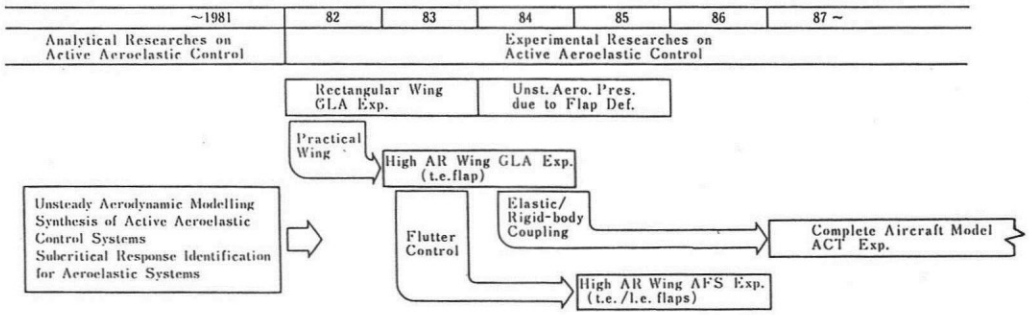

Fig.1 Research Program for Active Aeroelastic Control in NAL.

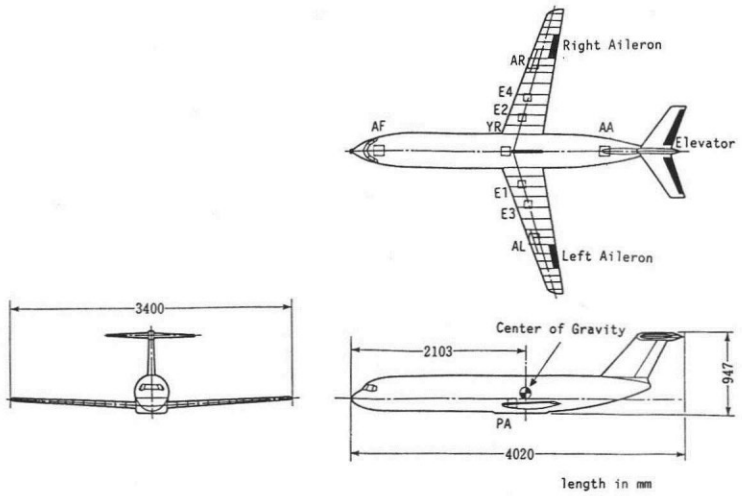

Fig.2 Three-View Drawing of ACT Model.

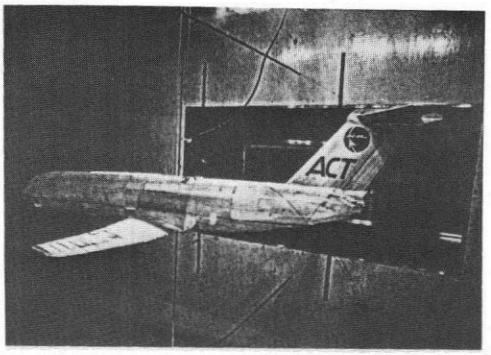

Fig.3 ACT Aircraft Model in GLA Experiment.

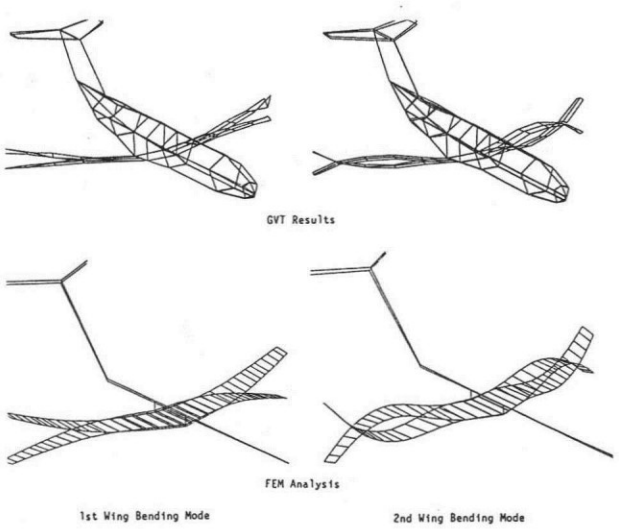

Fig.4 Typical Results of GVT and FEM Analysis.

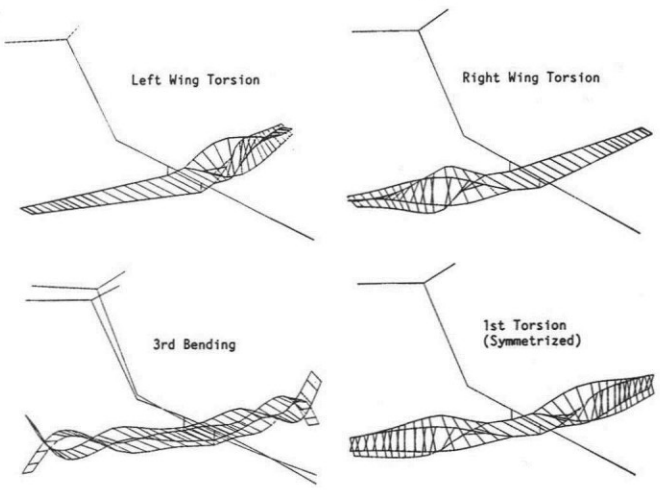

Fig.5 Higher Elastic Modes and Its Symmetrization.

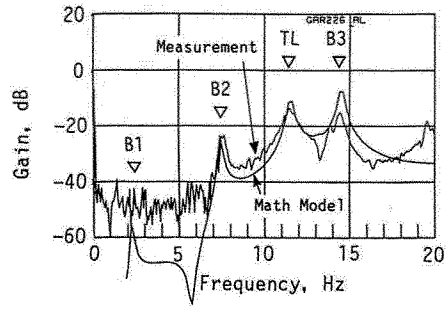

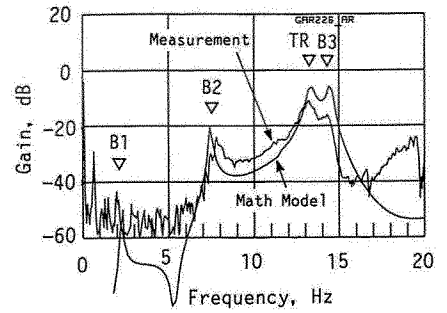

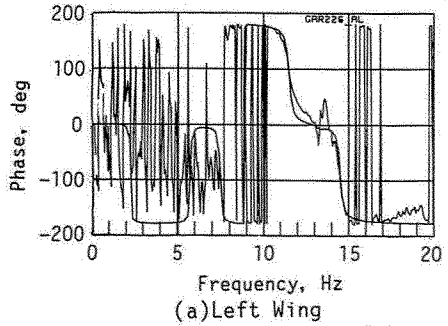

(a)Left Wing

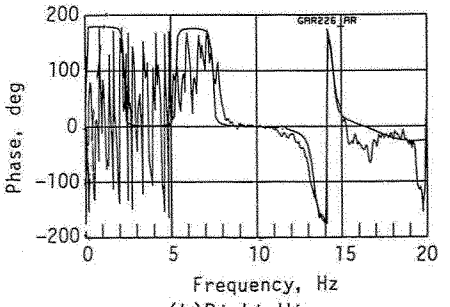

(b)Right Wing

Fig.6 Acceleration Response due to Aileron.

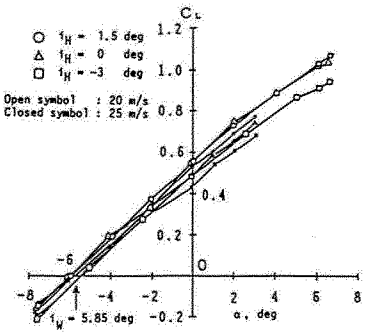

(a)$C_L \sim \alpha$ Diagram

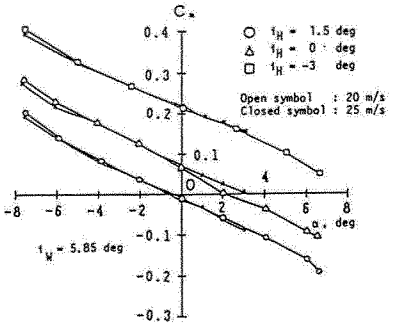

(b)$Cm \sim \alpha$ Diagram

Fig.7 Aerodynamic Measurement Results.

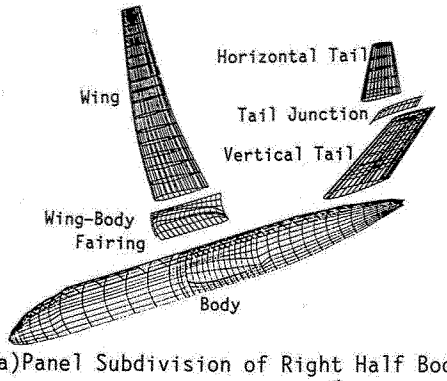

(a)Panel Subdivision of Right Half Body

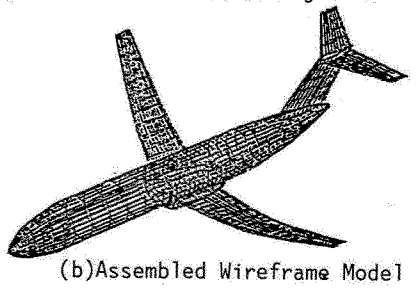

(b)Assembled Wireframe Model

Fig.8 Wireframe model for Static Aeroelastic Analysis.

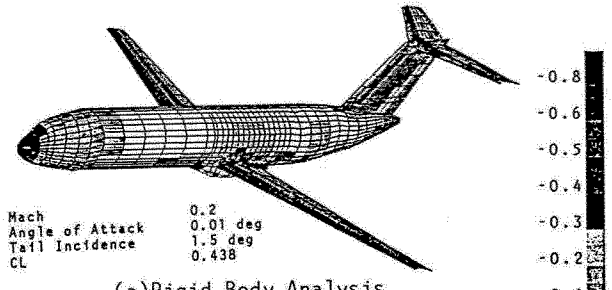

(a)Rigid Body Analysis

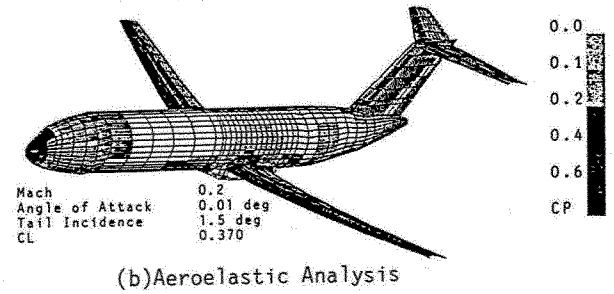

(b)Aeroelastic Analysis

Fig.9 Typical Pressure Distribution Obtained by Static Aeroelastic Analysis.

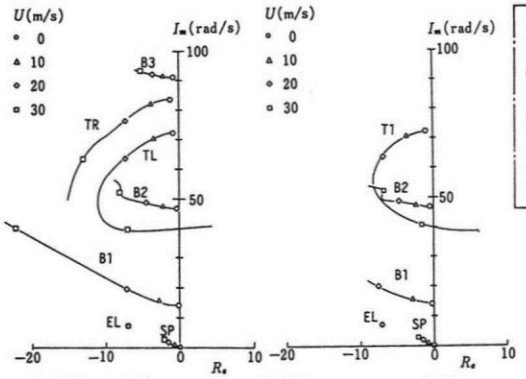

(a)Five Elastic Modes Model. (b)Symmetrized Elastic Mode Model.

Fig.10 Velocity Root Locus

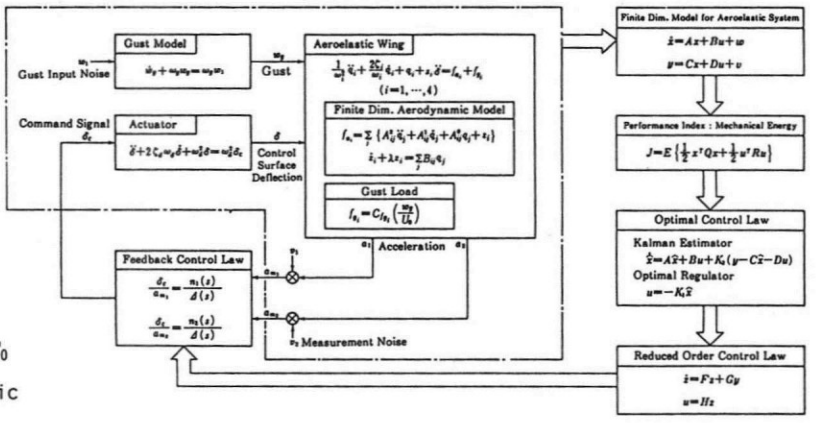

Fig.11 Control Law Synthesis Procedure for Active Aeroelastic Control.

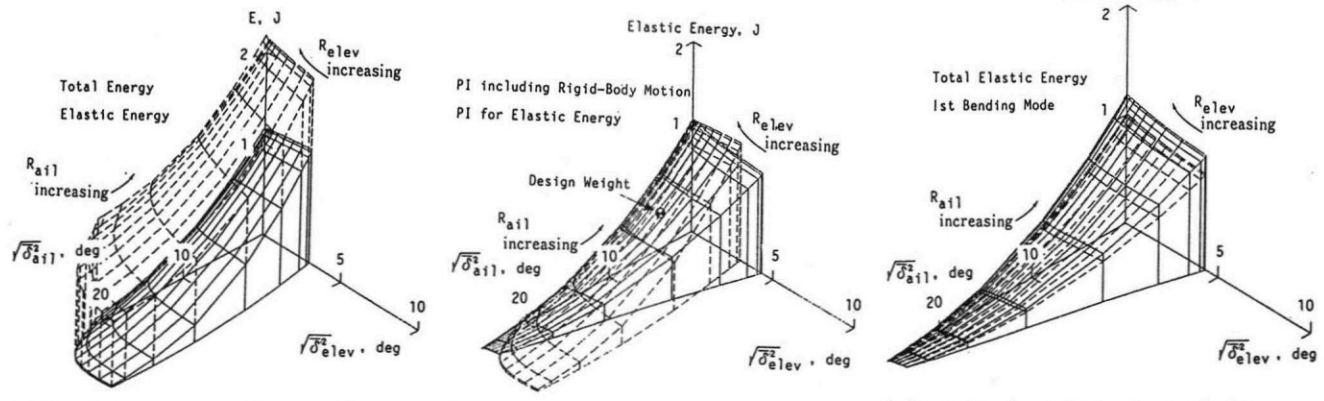

(a)Total Energy vs Elastic Energy (b)Total Energy Contribution to Elastic Energy (c)1st Bending Mode Contribution to Gust Load Alleviation.

Fig.12 Gust Load Alleviation Effectiveness of Aileron and Elevator.

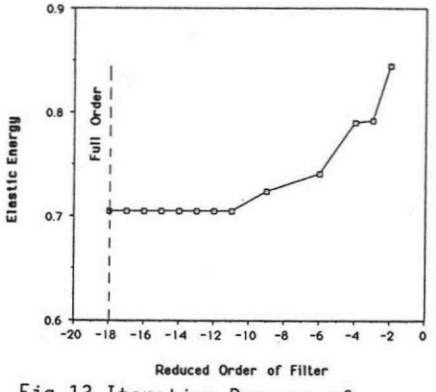

Fig.13 Iterating Process of Optimal Projection Algorithm.

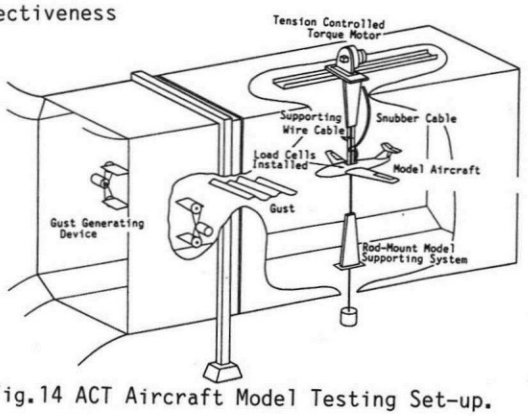

Fig.14 ACT Aircraft Model Testing Set-up.

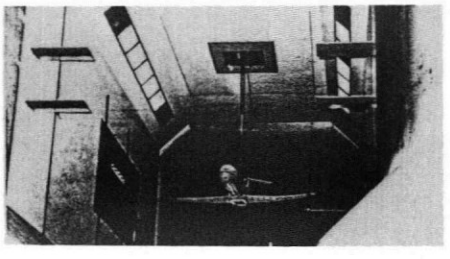

Fig.15 GLA Testing Set-up inside the Wind Tunnel.

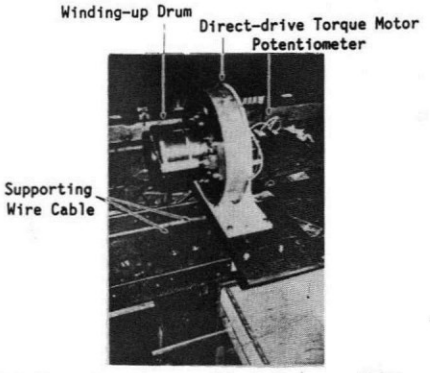

Fig.16 Tension Controlled Torque Motor.

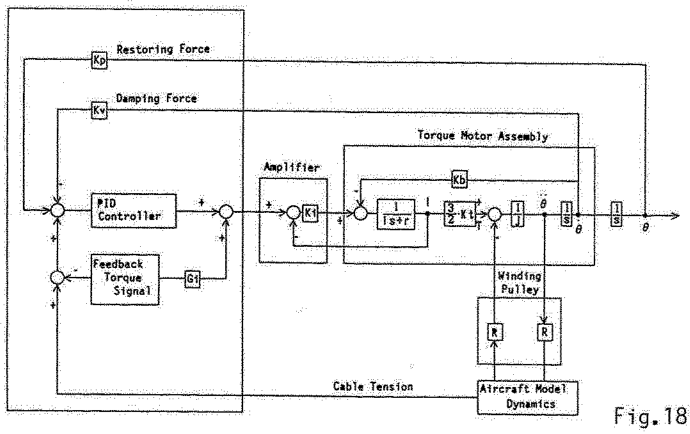

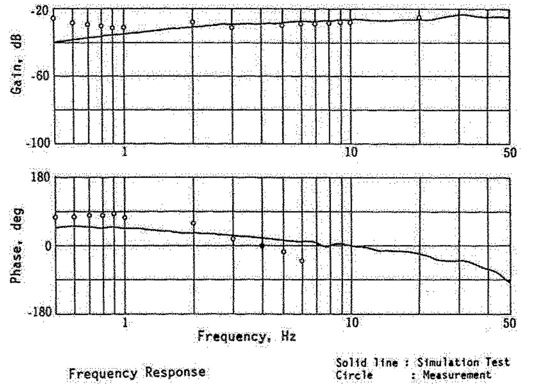

Fig.18 Frequency Response of the Model Supporting System.

Fig.17 Block Diagram of Tension Control Equipment.

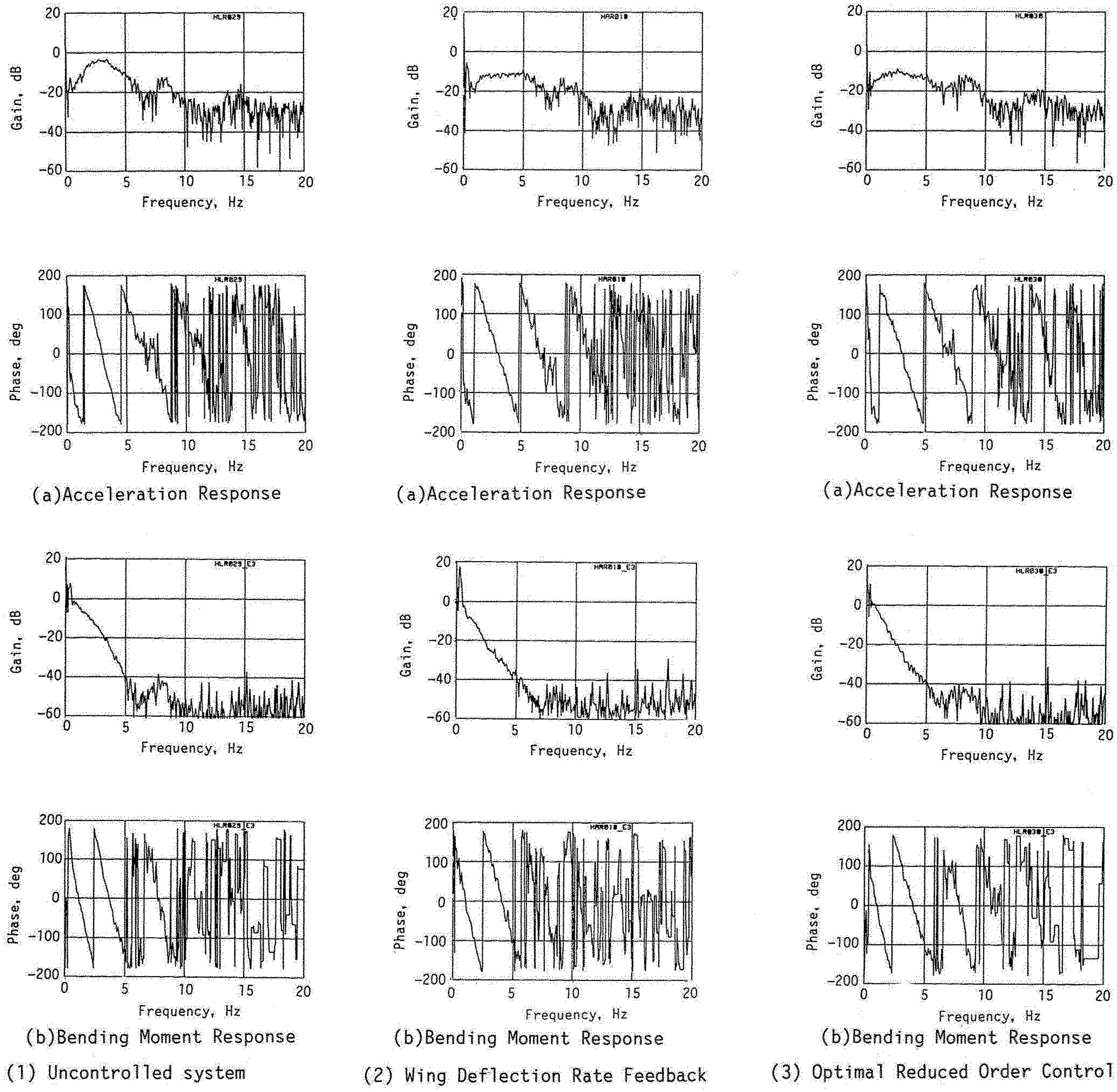

Fig.19 Experimental Results of Gust Load Alleviation.